Resolution improvement and noise reduction in human pinhole SPECT using a multi-ray approach and the SHINE method

A. Seret[1]; C. Vanhove[2]; M. Defrise[3]
[1]Imagerie médicale expérimentale, Université de Liège, Liège, Belgium; [2]Nuclear Medicine Department, University Hospital Brussels, Brussels, Belgium; [3]Nuclear Medicine Department, Vrije Universiteit Brussel, Brussels, Belgium

Keywords
Reconstruction pinhole SPECT, SPECT instrumentation, algorithms, thyroid

Summary
Purpose: This work aimed at quantifying the gains in spatial resolution and noise that could be achieved when using resolution modelling based on a multi-ray approach and additionally the Statistical and Heuristic Noise Extraction (SHINE) method in human pinhole single photon emission tomography (PH-SPECT). Methods: PH-SPECT of two line phantoms and one homogeneous cylinder were recorded using parameters suited for studies of the human neck area. They were reconstructed using pinhole dedicated ordered subsets expectation maximisation algorithm including a resolution recovery technique based on 7 or 21 rays. Optionally, the SPECT data were SHINE pre-processed. Transverse and axial full widths at half-maximum (FWHM) were obtained from the line phantoms. The noise was quantified using the coefficient of variation (COV) derived from the uniform phantom. Two human PH-SPECT studies of the thyroid (a hot nodule and a very low uptake) were processed with the same algorithms. Results: Depending on the number of iterations, FWHM decreased by 30 to 50% when using the multi-ray approach in the reconstruction process. The SHINE method did not affect the resolution but decreased the COV by at least 20% and by 45% when combined with the multi-ray method. The two human studies illustrated the gain in spatial resolution and the decrease in noise afforded both by the multi-ray reconstruction and the SHINE method. Conclusion: Iterative reconstruction with resolution modelling allows to obtain high resolution human PH-SPECT studies with reduced noise content. The SHINE method affords an additional noise reduction without compromising the resolution.

Schlüsselwörter
Bildrekonstruktion SPECT mit Pinhole-Kollimator, SPECT-Geräteausstattung, Algorithmen, Schilddrüse

Zusammenfassung
Ziel: Mit dieser Arbeit sollen die Verbesserungen der räumlichen Auflösung und des Bildrauschens quantifiziert werden, die mithilfe eines Bildauflösungsmodells auf der Grundlage des Mehrstrahl-Ansatzes zusammen mit der SHINE-Methode (Statistical and Heuristic Image Noise Extraction = statistische und heuristische Rauschunterdrückung bei bildgebenden Verfahren) bei der Einzelphotonen-Emissions-Tomographie mit Pinhole-Kollimator (PH-SPECT) am Menschen erreicht werden. Methodik: Es wurden PH-SPECT von zwei Linien-Phantomen und einem homogenen Zylinder-Phantom unter Verwendung von Parametern, die sich zur Untersuchung der menschlichen Halsregion eignen, aufgenommen. Sie wurden mit Hilfe des OS-EM (Ordered Subsets Expectation Maximisation)-Algorithmus mit Pinhole-Kollimator einschließlich einer auf 7 oder 21 Projektionsstrahlen basierten Wiederherstellungsmethode für die Auflösung rekonstruiert. Wahlweise wurden die SPECT-Daten zuvor mit der SHINE-Methode bearbeitet. Diagonale und axiale Halbwertsbreiten (Full Widths at Half-Maximum – FWHM) erhielt man durch die Linien-Phantome. Das Bildrauschen wurde mit dem Varianzkoeffizienten (Coefficient of Variation – COV) quantifiziert, der vom homogenen Phantom abgeleitet wurde. Mit denselben Algorithmen wurden zwei PH-SPECT-Untersuchungen der Schilddrüse am Menschen (ein heißer Knoten und eine sehr schlechte Aufnahme) bearbeitet. Ergebnisse: Je nach Anzahl der Iterationen verringerte sich die FWHM um 30 bis 50 %, wenn beim Rekonstruktionsprozess der Mehrstrahl-Ansatz verwendet wurde. Die SHINE-Methode hatte auf die Auflösung keine Auswirkungen, reduzierte jedoch den COV um mindestens 20 % und in Kombination mit der Mehrstrahl-Methode sogar um 45 %. Die zwei Untersuchungen am Menschen zeigen auf, welche Verbesserung bei der räumlichen Auflösung erreicht wurde und wie stark das Bildrauschen sowohl durch die Mehrstrahl-Rekonstruktion wie auch durch die SHINE-Methode reduziert werden kann. Schlussfolgerung: Eine iterative Bildrekonstruktion mit Bildauflösungsmodell ermöglicht eine hohe Auflösung bei PH-SPECT-Untersuchungen am Menschen bei gleichzeitig reduziertem Bildrauschen. Die SHINE-Methode erzeugt eine zusätzliche Rauschunterdrückung, ohne dabei die Auflösung zu beeinträchtigen.

Correspondence to:
Alain Seret,
Université de Liège, Imagerie médicale expérimentale,
Institut de Physique, B5, B-4000 Liège1, Belgium
Tel. +32/4/366 37 05, Fax +32/4/366 36 29
E-mail: aseret@ulg.ac.be

Tab. 1   Acquisition parameters for the phantom and patient data (projection matrix size 128×128; pinhole aperture diameter 5 mm)

phantom/patient	orbit extend	radius (cm)	tilt angle (°)	hardware zoom
2 lines	360°	5.8[a], 10.7	0	2
13 lines	180°	10.9	0, 20	1
cylinder	180°	11	0, 20	1
hot nodule patient	180°	12.3	22.8	1
low uptake patient	180°	10.2	24.7	2

[a] also with 3 mm pinhole aperture

In human, the pinhole collimator (PH) has been shown to allow single photon emission tomography (SPECT) of small field of views (FOV) with a higher spatial resolution than does the parallel hole collimators (15, 21, 24). However, PH and parallel hole collimators suffer from the same trade-off between resolution and sensitivity. For PH there is a supplementary trade-off between resolution and FOV size (2, 25):
- the higher the spatial resolution required,
- the smaller the pinhole aperture and
- the smaller the radius-of-rotation, and
- the smaller the FOV size.

Using either the point spread function (20) or a multi-ray technique (23), interesting improvements in resolution have been demonstrated for the small pinhole apertures (1–3 mm) and rotation radii (< 5 cm) used for small animal explorations. In addition, these resolution recovery techniques have the potential of decreasing the noise content of the reconstructed images. In human, PH-SPECT is generally applied with a 180° orbit instead of the 360° orbit used for small animals PH-SPECT and also with a larger rotation radius (6, 15, 21, 24). Moreover, for neck area exploration a moderately tilted detector is needed

to avoid the shoulders (6, 24). In addition, larger PH apertures (4–7 mm) are used to ensure reasonable sensitivity (6, 15, 21, 24). Nevertheless, the noise content of the image remains high.

Iterative reconstruction methods like the ordered subsets expectation maximisation (OSEM) have been advocated to replace the 3D filtered back-projection based algorithms (22, 27). Iterative techniques require a sufficient number of iterations to allow contrast recovery in all image areas with the concomitant drawback of increasing noise generation in the reconstructed slices (18). Human PH-SPECT would therefore largely benefit from resolution recovery techniques but also from any possible additional noise reduction method.

In this work, we explored OSEM reconstruction with multi-ray method in the framework of PH-SPECT performed with parameters suitable for human explorations: pinhole aperture of 5 mm, rotation radius of at least 10 cm and optional moderate (15–25°) tilt of the camera head. In parallel, the potential of the Statistical and Heuristic Noise Extraction (SHINE) method (7) to reduce the Poisson noise has also been explored.
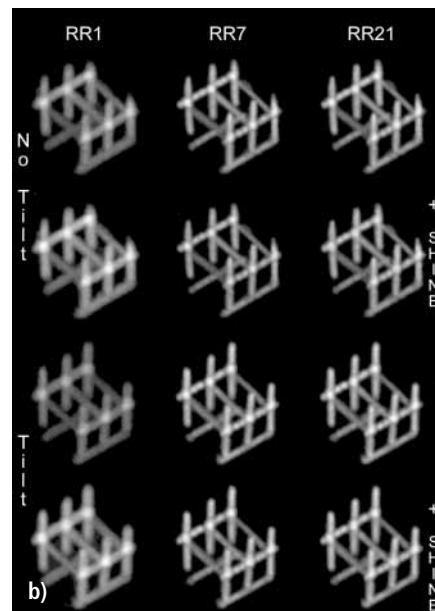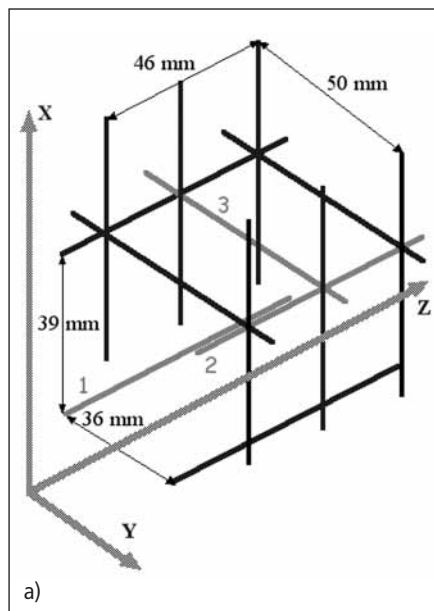
Material and methods

Acquisitions

All acquisitions were performed with a SMV DSX camera (Sopha Medical Vision, Buc, France). The pinhole collimator was a cone of 20.5 cm height and 29.5 cm base diameter. Its aperture diameter was 5 mm in all but one acquisition (line phantom, 360° orbit with the smallest radius) where the 3 mm-diameter aperture was also used. Single circular orbits were used. The orbit radius (R) is defined as the distance from the pinhole aperture to the camera axis of rotation (AOR). It was calculated from the camera rotation radius using the procedure previously described (15). R values were in the range 5.8 – 12.3 cm (▶Tab. 1). For acquisitions with a tilted camera head, the tilt angle (T) was read from the camera. T values were in the range 18.2° – 24.7° (▶Tab. 1). The energy window was centred at 140 keV for technetium-99m or at 159 keV for iodine-123 and extended over 20%. Projections were acquired in a 128×128 matrix.

Fig. 1   13-lines phantom
a) 3D sketch: Lines 1 and 2 were used to measure the resolution in the transverse plane and line 3 in the axial direction (z-axis) on the reconstructed images.
b) Maximum intensity projection views after 4 iterations: reconstruction with 8 subsets, eventually SHINE pre-processing of the projections (lines 2 & 4), and standard OSEM (RR1) or multi-ray OSEM with 7 (RR7) or 21 rays (RR21); camera head without tilt (lines 1 & 2) or with 20° tilt angle (lines 3 & 4)

Hardware zoom of two was used for some acquisitions (▶Tab. 1). 32 projections were recorded for 180° orbit and 64 projections for 360° orbit (▶Tab. 1). In order to avoid the additional artefact that could be generated by the incomplete 180° orbits and to get a point of comparison with previous works (15, 16, 22, 23), some acquisitions of the two lines phantom were performed with 360° orbits, no tilt and the smallest available pixel size (128×128 matrix and hardware zoom two) on the DSX camera. All other acquisitions used a 180° orbit.

Phantom studies

Two capillary line phantoms were used. Capillary inner diameter was 0.4 mm. The first one consisted in two parallel lines separated by (23.5 ± 0.5) mm (20.0 ± 0.5 mm horizontally and 12.5 ± 0.5 mm vertically). One line was positioned along and close to (within 1 mm) the AOR. The second line phantom (▶Fig. 1a) comprised 13 lines (16). The two base lines (lines lying in the Y, Z plane of ▶Figure 1a) and the AOR were in the same horizontal plane in such a way that the vertical plane containing the AOR was a mirror plane of the phantom. The AOR was identical to the z-axis in ▶Figure 1a. A Plexiglas cylindrical phantom of 70 mm inner diameter and 40 mm inner height was also used. It was filled with an aqueous solution of 185 MBq ^{99m}Tc and its axis was parallel and close to (within 5 mm) the AOR. The acquisition time per projection was set in order to accumulate at least 200 kcounts in each projection. All phantoms were filled with technetium-99m aqueous solutions.

Patient studies

A man (age: 52 years) with a single hot nodule on the thyroid right lobe was injected with 37 MBq iodine-123 and the acquisition was performed with steps of 50 s and no hardware zoom. A woman (age: 64 years) was injected with 180 MBq pertechnetate (^{99m}Tc). This patient demonstrated very low thyroid uptake. The acquisition was performed with steps of 40 s and a hardware zoom of two.

SHINE processing

SHINE processing of the projections was performed on a Segami Mirage workstation (Segami Corporation, MD). Interfile files were used to import to and export from this workstation. The SHINE method proceeds as follows (7). The noisy original image is divided into blocks of 4×4 pixels. Correspondence analysis is performed on the blocks, yielding 4×4 basis patterns called factors. Each block in the image is then reconstructed from the subset of factors that significantly contribute to the signal variance in that block. This subset is defined by assuming that the pixel variance within the block is equal to the sum of the signal variance and of the noise variance. Factors are added one by one to the subset until the residual variance, which is defined as the initial variance minus the reconstructed block variance, is found significantly lower than the noise variance using a classical variance comparison test. To avoid block artefacts, the procedure is repeated several times using a sliding window to divide the image into blocks. The final image is the mean of the images obtained for the various windows.

Reconstructions

Reconstructions were performed on a Macintosh iBook G4 laptop using the pinhole OSEM software described elsewhere (22, 23). In this software, the pinhole aperture is modelled as a geometrical point or as a circular aperture of finite size using a 7 or 21 rays method. Projections and backprojections are performed along these rays with a weighting factor. There is always one ray passing through the centre of the pinhole aperture. The 6 or 20 other rays pass through points regularly spaced along one (7 rays) or two (21 rays) circles centred on the pinhole aperture centre. The weighting factor depends only on the circle that the ray is crossing. No filter was applied prior to, during or after the reconstruction. There was no attempt to correct for attenuation or scatter. All reconstructions were performed without and with SHINE preprocessing of the projections. The subsets contained always four projections. Results will be given in term of equivalent number of MLEM iterations (iMLEM) calculated as the number of subsets times the number of iter-

ations. All data were reconstructed for iMLEM = 8, 16, 24, 32, 40 and 48. The software allowed free choice of the reconstructed voxel size. If not otherwise stated, isotropic voxels of 1 mm-side length were selected. Reconstructed data were automatically saved as transverse slices in Interfile 3.3 files.

Image analyses

A Medical Image Data Examiner (Amide, 0.8.19, Andy Loening) freeware running on the same Macintosh laptop was used for further analysis of the reconstructed images. The profile tool of this software was used to calculate the profile maximum and full width at half-maximum (FWHM) on capillary line images. The profile maximum position was taken as an estimate of the line position. The FWHM was measured on lines 1 and 2 in the two directions of the transaxial planes and on line 3 in the axial direction of the coronal planes (▶Fig. 1a). The FWHM measured in the transaxial planes were averaged for sake of clarity of the graphs. The ROI drawing and ROI statistics tools of AMIDE were employed to obtain mean and standard deviation in 3D regions of interest (ROI). For the cylinder phantom, the ROI was a cylinder of 12-mm tall and 40-mm diameter. For the hot nodule, a volume isocontour ROI was generated as follows. The reconstruction with the highest overall resolution (48 iMLEM) and SHINE pre-processing of the projections was selected and the isocontour threshold was set at 30% of the volume maximum. The ROIs were saved and automatically reported on all data sets obtained with the other reconstruction conditions. The standard deviation-to-mean ratio was defined as the coefficient of variation (COV) for the uniform cylinder phantom. For the hot nodule it could not be guaranteed that the iodine uptake in the selected area of the nodule was homogeneous. Therefore the standard deviation-to-mean ratio was not called COV.

Results
Reconstruction time

The total reconstruction time depended largely on the option used to model the pin-

hole aperture. With the laptop used and for the 180° orbit acquisitions (32 projections and 8 subsets), the following approximate values were observed. For the single ray option, the first iteration, which includes the computation of the OSEM normalisation matrix, lasted 30 s and each subsequent iteration needed 20 s. For the multi-ray options, the reconstruction times were one order of magnitude larger:

- 5 min with 7 rays or 9 min with 21 rays for the first iteration and
- 3 min with 7 rays or 5 min with 21 rays per subsequent iteration.

Phantom studies

For the 2 lines phantom, a 360° orbit and two radius (5.8 and 10.7 cm) were used. The dis-

tances between the lines measured on the reconstructed images were slightly lower than the true distances but the differences never exceeded 5%. For each line, each rotation radius and each reconstruction method, similar FWHMs were obtained along the x- and y-axis. The averaged x- and y-axis values (mean FWHM in the transaxial plane) are presented for the line located on the AOR and for the line located off-axis obtained for R = 6 and 11 cm (▶Fig. 2a). FWHM issued from the 7 and 21 rays method were in most cases so close to each other that the results for one of the methods was arbitrarily omitted from the graphs for sake of clarity. The acquisition with the shortest radius was repeated with the 3-mm aperture. These data were reconstructed with the single ray option and the FWHMs were measured (▶Fig. 2a). While nearly constant for the one ray method, the FWHM generally decreased with the increase in the number of iterations for the 7 and 21 rays methods. For R = 6 cm, the multi-ray method decreased the FWHM by 30% for iMLEM = 16 and up to 36 % for iMLEM = 48. For R = 11 cm, the decrease in FWHM amounted to 33% for iMLEM = 16 and up to 44 % for iMLEM = 48. Pre-processing of the projections with SHINE changed the reconstructed FWHM by less than 0.15 mm. It was observed that FWHM of the off-axis line (▶Fig. 2b) was lower than the FWHM of the on-axis line (▶Fig. 2a) especially for the shortest rotation radius.

For the 13 lines and the cylindrical phantoms, the orbits were limited to 180° and the radius was fixed at 11 cm. An acquisition was also performed with a camera head tilted by 20°. Reconstructed images of the 13 lines phantom are presented as 3D maximum intensity projection (▶Fig. 1b). The measured distances between any two lines of the phantom on the reconstructed images matched the true distances between these lines within 5% in the x- and y-directions and within 7% in the z-direction. FWHMs in the transverse plane were measured on lines 1 and 2 (▶Fig. 2c). Again, FWHMs issued from both multi-ray methods were so close to each other that the results for one of the methods were arbitrarily omitted from the graphs for sake of clarity. The higher the number of iterations, the lower the axial FWHM for the multi-ray methods (▶Fig. 3a). For the single ray method, the evolution of the FWHM with the
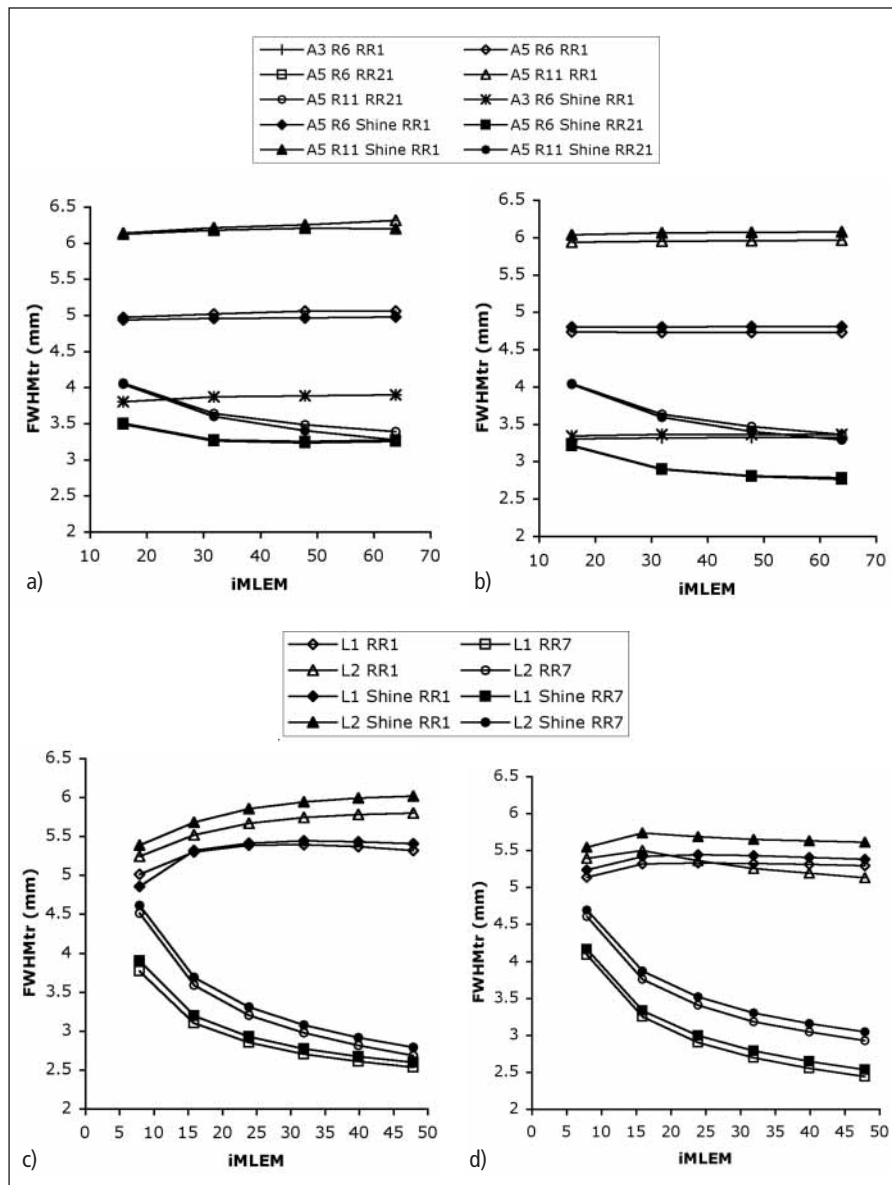

Fig. 2   Mean full width at half-maximum in the transverse plane; eventually SHINE pre-processing of the projections, and standard OSEM (RR1) or multi-ray OSEM with 7 (RR7) or 21 rays (RR21)
a, b) as a function of the number of equivalent MLEM iterations; acquisition parameters: 360° orbit, 64 projections (A: pinhole aperture in mm; R: pinhole radius in cm); reconstruction with 16 subsets, a) line on camera rotation axis; b) line off axis.
c, d) on line 1 (L1) or 2 (L2) of the 13-lines phantom as a function of the number of equivalent MLEM iterations; reconstruction with 8 subsets; c) no tilt, d) camera head tilted by 20°
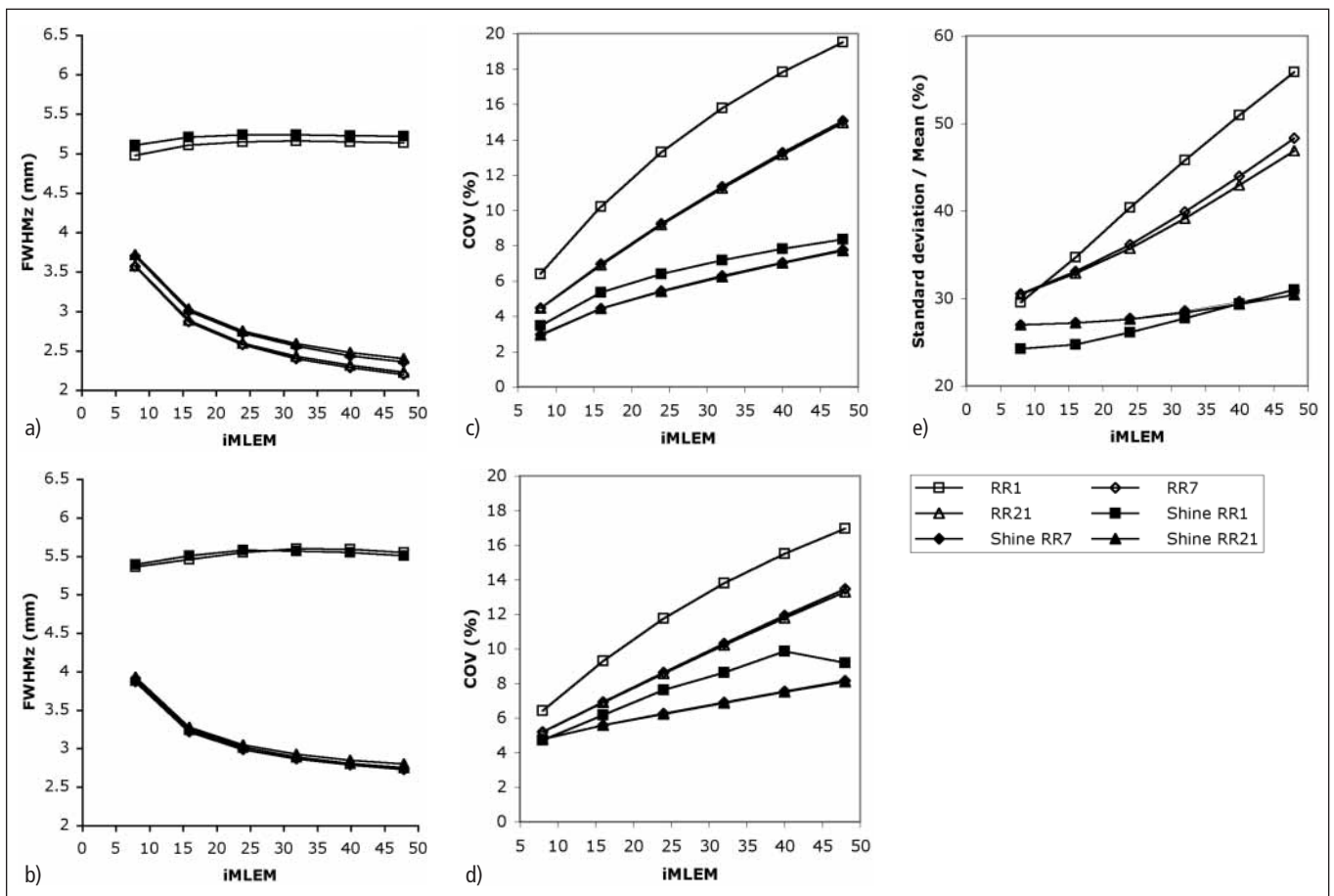
Fig. 3 Function of the number of equivalent MLEM iterations.; reconstruction with 8 subsets, eventually SHINE pre-processing of the projections, and standard OSEM (RR1) or multi-ray OSEM with 7 (RR7) or 21 rays (RR21); a, c) no tilt; b, d) camera head tilted by 20°

a, b) full width at half-maximum in the axial direction measured on line 3 of the 13-lines phantom

c, d) coefficient of variation measured on the cylinder phantom

e) standard deviation-to-mean ratio measured on a patient hot thyroid nodule

number of iterations was dependent on the line position and the direction. Preprocessing of the projections with SHINE changed the FWHM by less than 0.2 mm in most cases. The only exception was noticed for line 2 for which the transverse FWHM was increased by 0.4–0.5 mm (►Fig. 2d) when SHINE was applied to the projections acquired with the tilted camera. For iMLEM = 32, the decrease in FHWM obtained by the multi-ray methods exceeded generally 45%. The decrease in FWHM was limited for line 2 to 37% in the x-direction with the tilt.

The COV was measured over twelve consecutive reconstructed slices of the cylindrical phantom for acquisitions without and with a tilted camera head. The COV increased with the number of iterations (►Fig. 3c). The results for iMLEM = 32 were the followings.

The COV obtained with the single ray method applied to the raw projections amounted to 15.8% without tilt and to 13.8% with tilt. Reconstruction of the raw projections with the multi-ray methods reduced the COV to 11.2% without tilt and to 10.2% with the tilt. This corresponded to relative decreases in COV of 29% and 26%, respectively. Reconstruction with the single ray method of the SHINE preprocessed projections decreased the COV to 7.2% without tilt and to 8.6% with tilt. This corresponded to relative decreases in COV of 54% and 37%, respectively. Reconstruction with the multi-ray methods of the SHINE preprocessed projections decreased the COV to 6.2% without tilt and to 6.9% with tilt. This corresponded to relative decreases in COV of 60% and 50%, respectively.

For the other numbers of iterations considered in the study and when compared to the single ray method applied to the raw data, the multi-rays methods applied to the raw data afforded a relative decrease in COV of at least 20% and the multi-rays method applied to the SHINE preprocessed projections afforded a relative decrease of at least 45%.

Patient studies

The standard deviation-to-mean ratio was also measured on the reconstructed slices of a patient presenting a hot thyroid nodule (►Fig. 3e). The multi-ray methods reduced the ratio and SHINE preprocessing of the projections afforded a supplementary reduction of the ratio.
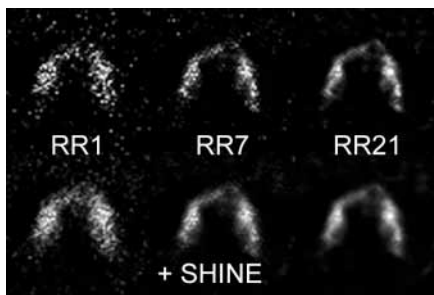
Fig. 4 Reconstructed coronal slice of the patient's thyroid with very low uptake obtained after 5 iterations with 8 subsets; from left to right: standard OSEM (RR1), multi-ray OSEM with 7 rays (RR7) or multi-ray OSEM with 21 rays (RR21); upper row: no pre-processing; lower row: SHINE pre-processing

A patient demonstrating a very low thyroid uptake was also imaged (▶Fig. 4). The impact of SHINE pre-processing of the projections is clearly highlighted as well as the benefit in resolution from the multi-ray method. In this patient, the 21 rays method allowed to obtain images of higher visual quality in spite of the very low number of acquired counts per pixel in the projections (a maximum of 10 counts was recorded in the hottest pixel of the anterior projection).

Discussion

Acquisitions parameters used in published patient studies of the neck area (6, 21, 24) were in the following ranges: 4 to 5 mm for the pinhole aperture diameter, 32 projections over 180° for the orbit angular extend, 8 to 15 cm for the rotation radius, 15 to 25° for the tilt angle. Depending on the camera used, the projection matrix was either 64×64 or 128×128 with or without hardware zoom. These values have guided the choice of the acquisition parameters made in this study (▶Tab. 1). The single orbit does not allow collection of data that satisfy the Tuy's condition (18, 23). However, many studies on small animals are performed with this kind of orbits and the OSEM algorithm allows to obtain from these imperfect data high quality reconstructed images (19, 25).

For both 360° and 180° orbits, the distance between the lines measured on the reconstructed images were very close to the true ones. The differences amounted to utmost

5% in the transaxial plane and to 7% in the axial direction. It should be noted that no sophisticated calibration procedure (3, 4) was used in this study. These small observed differences are comparable to those observed in previous works with the same equipment (15, 16).

Full 360° single circular orbit and a non-tilted camera head were used to obtain the projections of the 2 lines phantoms. For R = 6 cm, the single ray method allowed to obtain FWHM in the range 4.5–5 mm with the 5 mm pinhole aperture and in the range 3.5–4 mm with the 3-mm aperture (▶Fig. 2a). The multi-ray method decreased the FWHM obtained with the 5 mm aperture below the FWHM obtained with the 3 mm aperture and the single ray method (▶Fig. 2a). As this work aimed at acquisition parameters suitable for human studies, the multi-ray method was not applied to the 3 mm aperture acquisition. Even with R = 11 cm, the multi-ray method decreased the FWHM for the 5 mm aperture below the FWHM recorded for the 3-mm aperture and the smaller rotation radius of 6 cm (▶Fig. 2a). The FWHM appeared to be lower for the off-axis line than for the on-axis line (▶Fig. 2a). During the camera rotation, the line-to-pinhole opening distance was constant for the on-axis line but varied for the off-axis line. It resulted that this line provided higher counts with higher resolution near the collimator and lower counts with lower resolution far from the collimator. This could explain the FWHM differences observed between the two lines.

As discussed, the acquisition parameters used for the 13 lines phantom are typical of parameters suitable for explorations in humans. The rotation radius was of 11 cm and the acquisitions were performed without and with a tilted camera head. The tilt angle was fixed at 20°. The reconstructed images delivered by all reconstruction methods were of high quality (▶Fig. 1b). For the single ray method, the FWHM in the transverse plane (▶Fig. 2c, d) were similar to those obtained with the full 360° orbit and the same rotation radius (R = 11 cm). They were also very close to the FWHM measured with the same equipment and same acquisition parameters for this phantom in a previous work (16). Reconstruction with the multi-ray method decreased the FWHM by more than 30% for iMLEM equal to 16. When more iterations

were used, the decrease was higher and could amount to 50%. The multi-ray reconstruction technique delivered images with less noise content (▶Fig. 3c, d). This has been observed by others both in SPECT (with parallel [1, 26] and pinhole collimators [23]) and in PET (10, 11) when the detector point spread function is properly modelled.

The SHINE method (7) was chosen after a preliminary comparison of three noise reduction techniques:
- Gaussian post-filtering of the reconstructed images (15),
- Bayesian iterative reconstruction using the median root prior (18, 19) and
- SHINE.

SHINE demonstrated to be largely superior in effective noise reduction without nearly compromising the spatial resolution. Therefore the two other techniques were not further considered. The noise of SHINE processed projections is no more Poisson noise. We could observe this by applying SHINE to several intrinsic flood images of low numbers of counts per pixel obtained with the camera used in this study. The original pixel value distribution followed the Poisson law as expected. The SHINE processed images showed a distribution that was close to a Gaussian one. However, SHINE processed projections collected with parallel hole collimators have been reconstructed using OSEM without any detectable artefact (7).

For both line phantoms (▶Fig. 2), SHINE preprocessing of the projections had insignificant influence on the FWHM whatever being the orbit extent (180° or 360°) or the tilt angle of the camera head (no tilt or 20° tilt).

The reduction in noise afforded by resolution recovery in the reconstruction algorithm and by SHINE preprocessing of the acquired projections is clearly demonstrated on patient data (▶Figs. 3e and 4). The trends in the curves of the standard deviation-to-mean ratio against iMLEM (▶Fig. 3e) and in the curves of COV against iMLEM (▶Fig. 3c, d) were similar. The large improvement in image quality afforded by the multi-ray and SHINE methods is furthermore supported by images of the patient with a low thyroid uptake (▶Fig. 4). The images obtained without applying resolution recovery were of very poor quality, in contrast to the images obtained when using the multi-ray resolution recovery

method. Moreover, SHINE preprocessing of the projections allowed to reconstruct images with lower noise content, confirming the applicability of SHINE even on data with very poor counting statistics (7). However, the images of ▶ Figure 4 demonstrated a clear visual superiority of the 21-rays method over the 7-rays method. Such differences were not observed for the phantoms. This would recommend to use the 21-rays method for the study of more complex objects or of patients.

Several groups have demonstrated the clinical advantages of PH-SPECT for the study of thyroid and parathyroid glands, of lymph nodes and of small bones (5, 17). Most of these studies were performed with cameras from the eighties or the nineties. As pointed out in a recent publication (5), most of these groups, including ourselves, are actually facing a major difficulty: modern γ-cameras do not allow SPECT acquisition with a pinhole collimator and, or a tilted head. This comes mainly from a software limitation that the user can hardly overcome without an active support of the constructor. An easy solution to this problem would be the availability from the constructors of an optional package allowing PH-SPECT acquisitions. A longer but maybe more efficient way would be the development of a dedicated system. Such a system should ideally incorporate the latest developments in small-animal and human SPECT (14). For example, the multi-pinhole collimators allow superior sensitivity-resolution trade-offs (2, 12) and SPECT-CT has been shown interesting for the exploration of small organs like the parathyroid glands (8, 13). A high spatial resolution could also be very interesting in the field of the ablation of the thyroid remnant tissues with radioactive iodine. Indeed, it has been demonstrated that an accurate determination of the mass and the shape of these tissues was a critical point for the dosimetry to these tissues (9).

Conclusion

For the reconstruction of PH-SPECT data acquired in conditions representative of patient studies, an iterative algorithm (OSEM) including a multi-ray method led to large improvements (at least 30%) in the recon-

structed resolution. The preprocessing of the projections with the SHINE noise reduction technique did not alter the reconstructed resolution but improved the COV by at least 20%. When combining SHINE with the resolution recovery method, the COV was decreased by a minimum of 45%. Improvements in resolution and signal-to-noise ratio were illustrated with two human thyroid studies.

Conflict of interest
The authors declare, that there is no conflict of interest.

References

1. Bai C, Zeng GL, Gullberg GT et al. Slab-by-slab blurring model for geometric point response correction and attenuation correction using iterative reconstruction algorithms. IEEE Trans Nucl Sci 1998; 45: 2168–2172.
2. Beekman F, van der Have F. The pinhole: gateway to ultra-high-resolution three-dimensional radionuclide imaging. Eur J Nucl Med Mol Imaging 2007; 34: 151–161.
3. 3Béqué D, Nuyts J, Bormans G et al. Characterization of pinhole SPECT acquisition geometry. IEEE Trans Med Imaging 2003; 22: 599–612.
4. Béqué D, Nuyts J, Suetens P, Bormans G. Optimization of geometrical calibration in pinhole SPECT. IEEE Trans Med Imaging 2005; 24: 180–190.
5. Carlier T, Oudoux A, MiralliŽ E et al. 99mTc-MIBI pinhole SPECT in primary hyperparathyroidism: comparison with conventional SPECT, planar scintigraphy and ultrasonography. Eur J Nucl Med Mol Imaging 2008; 35: 637–643.
6. Desvignes P, Laurette I, Koulibaly PM et al. Evaluation clinique d'une méthode algébrique de reconstruction 3D pour la détection des nodules thyroïdiens froids par tomoscintigraphie sténopéïque. Médecine Nucléaire 2000; 24: 217–223.
7. Hannequin P, Mas J. Statistical and Heuristic Noise Extraction (SHINE): a new method for processing Poisson noise in scintigraphic images. Phys Med Biol 2002; 47: 4329–4344.
8. Krausz Y, Bettman L, Guralnik L et al. Technetium-99m-MIBI SPECT/CT in primary hyperparathyroidism. World J Surg 2006; 30: 76–83.
9. Grosev D, Loncaric D, Huic D, Dodig D. Geometric models in dosimetry of thyroid remnant mass. Nuklearmedizin 2008; 47: 120–126.
10. Panin VY, Kehren F, Michel C, Casey M. Fully 3-D PET reconstruction with system matrix derived from point source measurements. IEEE Trans Med Imaging 2006; 25: 907–921.
11. Qi J, Leahy RM, Cherry SR et al. High resolution 3D Bayesian image reconstruction using the micro-PET small animal scanner. Phys Med Biol 1998; 43: 1001–1013.
12. Rolleman EJ, Bernard BF, Breeman WAP et al. Molecular imaging of reduced renal uptake of radiolabelled [DOTA0,Tyr3]octreotate by the combination of lysine and Gelofusine in rats. Nuklearmedizin 2008; 47: 110–115.
13. Ruf J, Seehofer D, Denecke T et al. Impact of image fusion and attenuation correction by SPECT-CT on the scintigraphic detection of parathyroid adenomas . Nuklearmedizin 2007; 46: 15–21.
14. Seret A. Will high-resolution/high-sensitivity SPECT ensure that PET is not the only survivor in nuclear medicine during the next decade? Eur J Nucl Med Mol Imaging 2009; 36 533–535.
15. Seret A, Defrise M, Blocklet D. 180°Pinhole SPET with a tilted detector and OS-EM reconstruction: phantom studies and potential clinical applications. Eur J Nucl Med 2001; 28: 1836–1841.
16. Seret A, Flérès D, Defrise M. Body contour 180°pinhole SPET with or without tilted detector: a phantom study. Eur J Nucl Med Mol Imaging 2003; 30: 1205–1210.
17. Seret A, Hustinx R. Clinical applications of pinhole single photon emission tomography. Current Medical Imaging Reviews 2006; 2: 347–352.
18. Sohlberg A, Ruotsalainen U, Watabe H et al. Accelerated median root prior reconstruction for pinhole single-photon emission tomography (SPET). Phys Med Biol 2003; 48: 1957–1969.
19. Sohlberg A, Lensu S, Jolkkonen J et al. Improving the quality of small animal brain pinhole SPECT imaging by Bayesian reconstruction. Eur J Nucl Med Mol Imaging 2004; 31: 986–994.
20. Sohlberg A, Watabe H, Zeniya T, Iida H. Comparison of multi-ray and point-spread function based resolution recovery methods in pinhole SPECT reconstruction. Nucl Med Commun 2006; 27: 823–827.
21. Spanu A, Falchi A, Manca A et al. The usefulness of neck pinhole SPECT as a complementary tool for planar scintigraphy in primary and secondary hyperparathyroidism. J Nucl Med 2004; 45: 40–48.
22. Vanhove C, Defrise M, Franken PR et al. Interest of the ordered subsets expectation maximization (OS-EM) algorithm in pinhole single-photon emission tomography reconstruction: a phantom study. Eur J Nucl Med 2000; 27: 140–146.
23. Vanhove C, Andreyev A, Defrise M, et al. Resolution recovery in pinhole SPECT based on multi-ray projections: a phantom study. Eur J Nucl Med Mol Imaging 2007; 34: 170–180.
24. Wanet P, Sand A, Abramovici J. Physical and clinical evaluation of high-resolution thyroid pinhole tomography. J Nucl Med 1996; 37: 2017–2020.
25. Weber DA, Ivanovic M. Ultra-high-resolution imaging of small animals: Implications for preclinical and research studies. J. Nucl Cardiol 1999; 6: 332–344.
26. Zeng GL, Gullberg GT, Tsui BMW, Terry JA. Three dimensional iterative reconstruction algorithms with attenuation and geometric point response correction. IEEE Trans Nucl Sci 1991; 38: 693–702.
27. Zeniya T, Watabe H, Aoi T et al. A new reconstruction strategy for image improvement in pinhole SPECT. Eur J Nucl Med Mol Imaging 2004; 31: 1166–1172.